

Retinal Vessel Segmentation Using Parallel Grayscale Skeletonization Algorithm and Mathematical Morphology

Jardel Rodrigues, Nivando Bezerra
Departamento da Telemática
Instituto Federal de Educação, Ciência e Tecnologia do Ceará
Fortaleza, Brasil
jardel.rodrigues@ppgcc.ifce.edu.br, nivando@ifce.edu.br

Abstract—Retinal vessel segmentation is an important step for the detection of numerous system diseases, such as glaucoma, diabetic retinopathy, and others. Thus, the retinal blood vessel analysis can be used to diagnose and to monitor the progress of these diseases. Manual segmentation of fundus images is a long and tedious task that requires a specialist. Therefore, many algorithms have been developed for this purpose. This paper demonstrates an automated method for retinal blood vessel segmentation based on the combination of topological and morphological vessel extractors. Each of these extractors is based on different blood vessel features to increase the detection robustness. The final segmentation is obtained intersecting the two resulting images, smoothing the vessel borders and removing spurious objects remaining. Our proposed method is tested on DRIVE and STARE databases, achieving an average accuracy of 0.9565 and 0.9568, respectively, with good values of sensitivity and specificity.

Keywords—retinal blood vessel segmentation; mathematical morphology.

I. INTRODUCTION

Retinal fundus images provide an effective way to study and diagnose the health of optic nerve, vitreous, macula, retina, and blood vessels. In particular, the retinal blood vessels may provide important information about several system diseases, such as glaucoma [1], stroke, arteriosclerosis [2], arterial hypertension, heart diseases, and diabetic retinopathy [3]. Early detection allows the patients to treat themselves before the disease can advance and avoid more serious complications, like tunnel vision or even total blindness, in case of diabetic retinopathy [4]. For these reasons, the segmentation of retinal images is an important tool for pathologies monitoring and other applications. The retinal blood vessels and the main structures of a typical fundus image is depicted in Fig. 1. The blood vessels originate from the center of the optic disk, spread over the retina, and are responsible for supplying the blood throughout the entire region. Also, they transmit information signals from the retina to the brain [5].

The manual segmentation of retinal images is a long and tedious task that requires a specialist [4]. In order to overcome this situation, the development of computer aided systems is necessary for this scenario and several methodologies have been developed for this purpose. A large number of algorithms

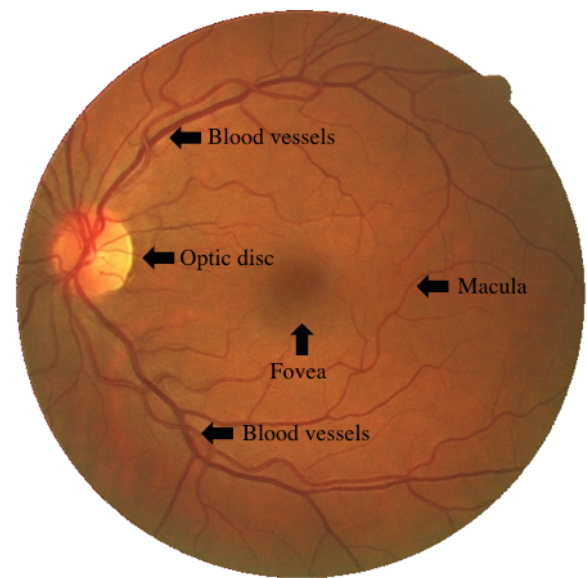


Fig. 1. A typical example of retinal fundus image showing main features of retina

and techniques have been published relating to the retinal blood vessels segmentation [6]. But, the accurate blood vessel segmentation is still a difficult task. The main obstacles are the presence of noise, low contrast, poor quality of some images, and anatomical variability of the vessels. For example, two close vessels are often considered as one wide vessel. In contrast, a vessel with central light reflex may be misunderstood as two vessels [7].

This work proposes a novel approach to segment the retinal blood vessels using extractors that preserves their topological properties and connectivity. Several methods that use the vessel skeletons can be found at literature [6], [8]. The main novelty of our method is to employ a parallel grayscale skeletonization algorithm alongside morphological operations to provide a viable solution to reach our goal. Our method achieves significant results and obtains competitive measurements in terms of accuracy and specificity against several

State-of-the-art models. In particular, we outperformed these measurements in two widely used databases, namely, DRIVE and STARE. According to the obtained results, the developed method presented robustness to the typical problems of this kind of images.

II. RELATED WORK

We provide here a brief review, categorization and analysis of unsupervised methods for retinal blood vessel segmentation. Several methods the detection of retinal blood vessels are reported in the literature; so far, it has remained a non-trivial problem. Authors often classify the segmentation techniques in unsupervised and supervised methods [3] [6] [9]. The unsupervised methods work without prior knowledge of labels. They can utilize several techniques, such as matched filtering [10], multiscale approaches [11], mathematical morphology [8], fuzzy c-means clustering [12], and vessel tracing/tracking [13]. On the other hand, the supervised methods exploit some prior labeling information to decide whether a pixel belongs to a vessel or not. However, we recall that such methods require label data that, in most cases, might not be present [6]. Some approaches fit in this category by using artificial neural networks and backpropagation algorithms [14], support vector machines (SVM) [15], principal component analysis (PCA) [16], and Gaussian mixture model (GMM) [17]. Our method is categorized in the unsupervised category, i.e., we do not utilize any labelling information.

Mendonça and Campilho [8] proposed a vessel segmentation algorithm which combines differential filters, for centerlines extraction, with morphological operators, used for filling vessel segments. The intensity and the morphological properties of vascular structures, such as linearity, connectivity, and width are considered in this approach. The segmentation algorithm is divided into three main steps: 1) The image is preprocessed for background normalization and a multiscale morphological enhancement technique is employed to improve the contrast of the blood vessels; 2) Four directional differential operators are applied and their outputs are processed in order to select connected sets of candidate points to be further classified as centerline pixels using vessel derived features; 3) The final segmentation is obtained by an iterative region growing method that integrates the contents of several binary images from vessel width dependent morphological filters.

Martinez-Perez et al. [11] presented a method based upon multiscale feature extraction. The scale-space analysis concerning the width approximation, size, and orientation from retinal blood vessels, is obtained by using two geometric features: gradient magnitude and maximum principal curvature of the Hessian tensor. These geometric features are based upon the first and the second spatial derivatives of the intensity calculated for each different scale that gives information about the topology of the image. Then, the authors used a multiple pass region growing procedure that progressively segments the blood vessels using the feature information alongside spatial information about the eight-neighbouring pixels, resulting in

a segmented binary image. The algorithm is tested with both red-free fundus images and fluorescein angiograms.

Yang et al. [12] proposed an automatic-hybrid method comprising of two steps that combine mathematical morphology and a fuzzy clustering algorithm. In the first step, linear structuring elements at various orientations are used according to the line type property of vessels. These structuring elements are applied to perform an opening operation to smooth the reversed color image. After the image has been smoothed, the top-hat transformation is applied to strengthen the vessels in the image. In that case, appropriated structuring elements are used in various directions in order to increase the gray difference between vessels and the background. After the retinal vessel enhancement, the vessel extraction takes place in the process through a fuzzy clustering algorithm followed by a purification procedure.

Zhang et al. [10] proposed a novel extension of zero mean Gaussian filter approach, namely Matched Filter with First-Order Derivative of the Gaussian (MF-FDOG), for retinal blood vessel segmentation. The traditional matched filter (MF) is a simple, and yet effective, method for vessel extraction, but it responds also to non-vessels and edges. The authors considered that the cross section of a vessel is a symmetric Gaussian function. Thus, it is employed a pair of filters, the MF and the first-order derivative of the Gaussian (FDOG), to detect the vessels. Around the pixel position, the true vessels have a strong response to the MF and the local mean of its response to the FDOG is close to zero. For non-vessel structures, both the responses are high. This way, the difference implies that vessels and non-vessels edges can be better distinguished by using the MF-FDOG than the traditional MF. At the end, the vessel map is detected by applying a threshold T to MF response map, while the threshold T is adjusted by FDOG response map so as to remove the non-vessels edges and extract the thin vessels.

In the Lam et al. [18] proposal, a novel multiconcavity modeling approach is developed to segment both healthy and unhealthy retinas. Three different concavity measures are proposed to detect blood vessels and each measurement addresses the negative impact produced by the lesions for identifying the normal vessels. The authors proposed a perceptive transform to model human visual perception in retinal image analysis using Weber's law [19]. They explored the fact that the bright lesions can be distinguished from the vessels and non-vessels by measuring the degree of concavity based on differentiability because the bright lesions have a steep intensity transition pattern. The dark lesions have an irregular shape intensity structure while blood vessels have a line-shape intensity structure. A line-shape concavity detection method is developed to prune the dark lesions while keeping the line-shape blood vessels. A locally normalized concavity detection method is proposed to normalize the strengths of noise removal in different regions due the fact that retinal image has a spherical intensity variation. At the end, these concavity measurements are combined according to their statistical and geometrical properties.

Fraz et al. [6] obtained the skeleton of the blood vessels by the detection of vessel centerlines while the vessel shape and orientation map are produced by morphological bit planes slicing. The centerlines are extracted by using the first order derivative of a Gaussian filter in four orientations and then, the evaluation of derivative signs and average derivative values is carried out. The shape and the orientation map of blood vessels are obtained by applying a multidirectional morphological top-hat operator with a linear structuring element followed by bit plane slicing of the vessel enhanced grayscale image. The segmented vessel tree is generated by the reconstruction of the vessel centerlines image with the vessel shape and orientation map.

III. PROPOSED METHOD

We propose a segmentation method whose its capability is based on a combination of two different vessel extractors: a topological and a morphological one. Each extractor aims different vessel features. The topological extractor focuses on connectivity and the morphological extractor focuses on vessel segment length. The obtained vessel networks from each extractor are combined in order to form a single network. The combined network is smoothed and spurious objects are removed to improve the segmentation result. A schematic overview is shown in Fig 2.

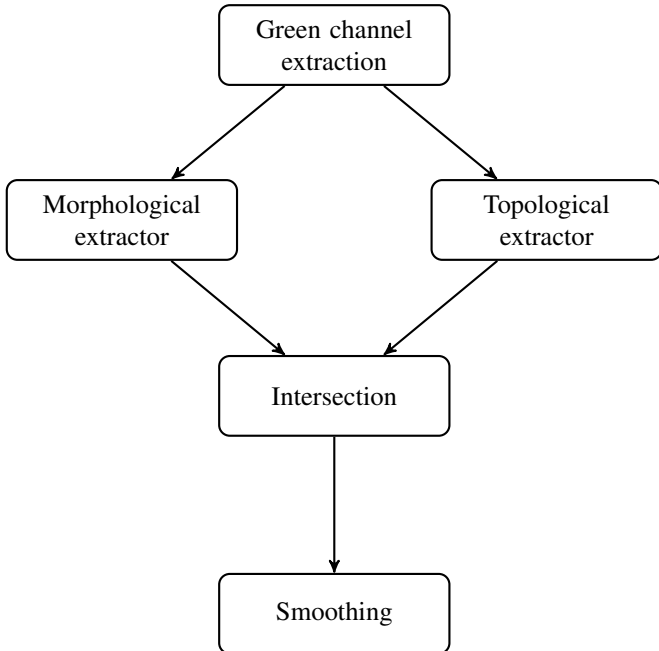


Fig. 2. Vessel segmentation method

A. Green channel extraction

Initially, we extract the green channel from the RGB image I in order to get the maximum contrast between the vessels and the background to compose our initial image I_g , as in Aramesh and Faez [20].

B. Morphological extractor

The morphological top-hat transform is used to extract the blood vessels, making an initial vessel tree. The top-hat transform is given by:

$$I_t^\theta = I_g - \gamma_\theta(I_g), \quad (1)$$

where I_g is the image green channel and $\gamma_\theta(I_g)$ is a morphological opening with linear structuring element oriented at each θ degrees performed on green channel image with length l . The structuring element length is chosen according to the size of the vessels for each dataset. This operation produces an image with an enhanced vessel structure. The sum of top-hat along each direction enhances the vessels regardless of their direction. The sum is depicted by:

$$I_\Sigma = \sum_{\theta \in A} (I_t^\theta), \quad (2)$$

where I_t^θ is the result of the top-hat performed with the structuring elements. The set A can be defined as $\{x \mid 0 \leq x \leq 180 \text{ and } x \bmod(22.5) = 0\}$. Later, the image is binarized using a threshold value t , resulting in an image I_b . A low threshold value is adopted to maximize the detection of vessel pixels. To summarize, our morphological extractor is composed by these three operations, the top-hat transform, the sum of top-hats and the binarization.

C. Topological extractor

The skeletonization algorithm presented by Couprie et al. [21] is an alternative to traditional skeletonization following a binarization. It allows reducing the blood vessels to thin lines in gray level space. This is important because retinal images are noisy, what makes finding a global thresholding for binarization a difficult task. The topological vessel extraction focuses on connectivity features to obtain a vessel network. A common approach in image processing consists in the segmentation of the object of interest followed by the use of a thinning operation to produce a skeleton. This skeleton is composed of thin line segments with the same connectivity and topology from the initially segmented object. The success of this kind of approach relies on the segmentation quality. Unfortunately, as we already discussed, the quality of retinal images is low.

Instead, we avoid the initial segmentation step and use directly the grayscale image. The thinning algorithm lowers the pixels gray levels respecting a simple connectivity pattern. The result is an initial grayscale skeleton image where the thin bright patterns are preserved and dark areas are thickened. A further contrast criterion c is employed to eliminate some spurious branches. The optimal value c is found using a grid search on the interval (1, 8). After thinning, a crest line detector produces a binary skeleton corresponding to the local brighter thin lines in the grayscale skeleton. Then, the skeleton image is dilated with a disc shaped structuring element. The radius of the structuring element is adjusted in accordance with

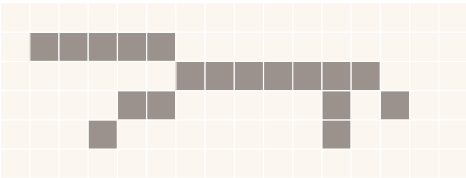
the vessels width. The dilation is depicted by:

$$I_\delta = \delta(I_s), \quad (3)$$

where $\delta(I_s)$ represents the dilation performed on skeleton image. This last operation makes the width of the vessels equals to the larger ones [22]. The Fig. 3 illustrates the process. We note the robustness of the crest line extraction since the binary skeleton in Fig. 3 (b) cannot be trivially obtained by a single thresholding of the Fig. 3 (a).

0	0	0	0	0	0	0	0	0	0	0	0	0	0	0	0
0	2	9	9	7	7	8	5	3	0	0	0	0	0	0	0
0	0	1	1	1	3	8	8	8	5	4	2	2	1	0	0
0	0	0	0	2	7	2	8	1	1	0	1	0	2	0	0
0	0	0	1	0	0	0	0	0	0	0	1	0	0	0	0
0	0	0	0	0	0	0	0	0	0	0	0	0	0	0	0

(a) grayscale skeleton



(b) thinning and crest line detection

Fig. 3. Topological vessel network extraction

D. Intersection

The fourth step of our method consists in the intersection of the two images: morphological and topological vessel networks. The resulting intersection of these two images compose our preliminary vessel tree. The intersection of these images is given by:

$$I_\cap = I_b \cap I_\delta, \quad (4)$$

where I_b represents the sum of top-hat binarized image and I_δ represents the dilated skeleton image. The intersection eliminates the noise and part of spurious objects. Thus, the undesired information that appears in the sum of top-hat image does not appears in the dilated skeleton image, and vice versa.

E. Smoothing

The final step of the method consists of two main operations. The first operation is the vessel border smoothing. This operation makes the segmented vessels have the shape of the manual segmentation, increasing the resulting quality. For smoothing, we use a morphological opening operation with disc shaped structuring element s . The second operation is the spurious objects elimination. The final segmentation I_Ω is obtained by eliminating small objects that have fewer than p pixels by using an area opening operation [23]. The values of these two parameters are found empirically by analysis of the image features. The segmentation results of each step are shown in Fig. 4.

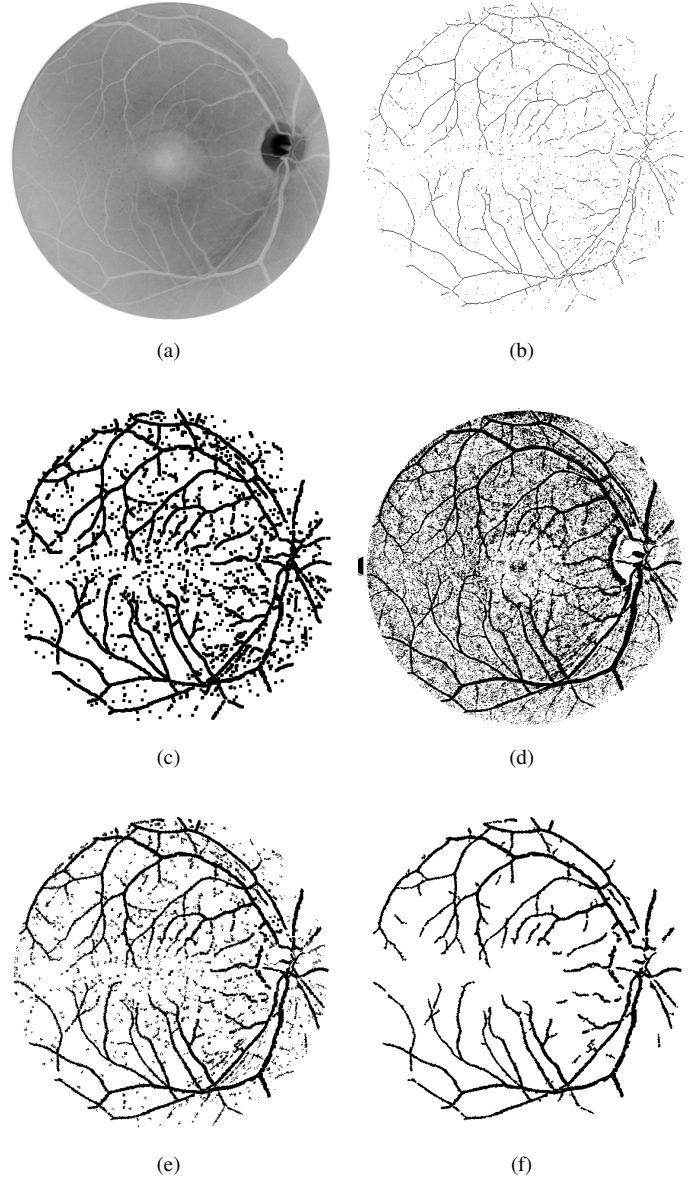


Fig. 4. Input image and outputs of segmentation steps. (a) Green channel of fundus image. (b) Result of parallel grayscale skeletonization algorithm. (c) Dilated skeleton. (d) Binarized sum of top-hat. (e) Intersection. (f) Final segmentation

IV. EXPERIMENTS

In this section, we present the databases on which the retinal vessel segmentation algorithms were evaluated, the performance measures adopted and the obtained results.

A. Databases

The Digital Retinal Images for Vessel Extraction (DRIVE) [24] is a publicly available database, consisting of a total of 40 color fundus eye photographs. The photographs were obtained from a diabetic retinopathy screening program in the Netherlands. The screening population consisted of 400 diabetic subjects between 25 and 90 years of age. Forty

photographs have been randomly selected, 33 do not show any sign of diabetic retinopathy and 7 show signs of mild early diabetic retinopathy. The set of 40 photographs was divided into a test and training set both containing 20 images. There are two hand-labeling available for each test image by two different human observers. The manually segmented images by 1st observer are used as ground truth and the segmentations of 2nd observer are tested against the 1st observer, serving as a human observer reference for performance comparison truth [25]. The performance of the vessel segmentation algorithms is measured on the test set [6].

The STructured Analysis of Retina (STARE) database [25] was conceived and initiated in 1975 by Michael Goldbaum, M.D., at the University of California, San Diego. The full set contains 400 images, which 40 are used for blood vessel segmentation and 10 of these contain pathology. Of these, two observers manually segmented all the images. The 1st observer segmented 10.4% of pixels as vessel, against 14.9% vessels for the 2nd observer. The difference in segmentation between the two observers is due to the fact that the 2nd observer segmented thinner vessels. The manually segmented images by 1st observer are used as ground truth and the human observer reference is obtained using the 2nd observer against the 1st observer.

B. Experiments setup

The mask is a binary image with the same resolution as that of fundus image. Pixels belonging to the fundus are marked with ones and the background of the fundus with zeros [26]. The fundus mask for each image is used to remove the background noise by multiplying the mask by the original image and to delimit the region of interest (ROI). The fundus mask for the DRIVE images are already available in the dataset, but the STARE database does not offer the masks. Thus, for each original image of this database, we created a fundus mask using the Hue, Saturation, and Intensity (HSI) color. The intensity channel image is thresholded with a low threshold value to produce the mask since the background pixels are significantly darker than the fundus pixels.

C. Performance measurements

The performance measures are obtained by the pixel-based classification result. Pixels in the segmented image can be classified as a vessel or a non-vessel. There are four possible classifications. Two of them are correct classifications and two are misclassifications. The correct classifications are the True Positive (TP) and True Negative (TN) and the two misclassifications are the False Negative (FN) and the False Positive (FP). These terminologies are shown in Table I.

TABLE I
TERMINOLOGIES IN VESSEL CLASSIFICATION.

	Vessel Present	Vessel Absent
Vessel detected	True Positive (TP)	False Positive (FP)
Vessel not detected	False Negative (FN)	True Negative (TN)

Our method is evaluated in terms of accuracy, sensitivity, and specificity. The accuracy is measured by the ratio of the total number of correctly classified pixels (sum of true positives and true negatives) by the number of pixels. The sensitivity is the ability of the algorithm to detect the vessel pixels and the specificity is the ability of the algorithm to detect non-vessel pixels. These performance metrics are defined in Table II based on the terms in Table I.

TABLE II
PERFORMANCE METRICS FOR VESSEL SEGMENTATION.

Measure	Description
Accuracy	$(TP + TN)/(TP + FP + TN + FN)$
Sensitivity	$TP/(TP + FN)$
Specificity	$TN/(TN + FP)$

Other performance metrics are also considered in our evaluation, such as False Positive Rate (FPR), False Negative Rate (FNR), Positive Predictive Value (PPV), Negative Predictive Value (NPV) and Matthew's Correlation Coefficient (MCC). The False Positive Rate (FPR) gives the percentage of pixels erroneously detected as vessel pixels. The False Negative Rate (FNR) gives the percentage of pixels erroneously detected as non-vessel pixels. The Positive Predictive Value (PPV) is the probability that an identified vessel pixel is a true positive. It gives the proportion of the identified vessel pixels which are true vessel pixels. The Negative Predictive Value (NPV) is the probability that an identified non-vessel pixel is a true negative. It gives the proportion of the identified non-vessel pixels which are true non-vessel pixels. Finally, the Matthew's Correlation Coefficient (MCC) is used in machine learning and is a measure of the quality of binary (two-class) classification. The coefficient can assume any value in the interval between -1 and +1. A value of -1 indicates a total disagreement between prediction and observation, 0 no better than random prediction and +1 indicates a perfect prediction.

These performance metrics are not available for most of the published methods and are summarized in Table III.

TABLE III
ADDITIONAL PERFORMANCE METRICS FOR VESSEL SEGMENTATION.

Measure	Description
FPR	$FP/(FP + TN)$
FNR	$FN/(TP + FN)$
PPV	$TP/(TP + FP)$
NPV	$TN/(TN + FN)$
MCC	$\frac{TP \times TN - FP \times FN}{\sqrt{(TP+FP)(TP+FN)(TN+FP)(TN+TN)}}$

V. RESULTS AND DISCUSSION

Our method is evaluated on both DRIVE and STARE databases. The 20 images of the test set with their respective ground truth segmentation were used in our experiment. All the State-of-art methods used only the test set. Thus, our proposal has been limited to use this set of images.

A. Evaluation

In Tables IV and V is shown the performance of surveyed method against ours. The results were extracted directly from the original papers.

TABLE IV
AVERAGE PERFORMANCE RESULTS FOR DRIVE DATABASE.
(PARAMETERS: $l = 19$; $t = 44$; $c = 6$; $s = 3$; $p = 60$).

Methodology	Accuracy	Sensitivity	Specificity
Proposed method	0.9565	0.7323	0.9783
Lam et al. [18]	0.9472	-	-
2nd human observer	0.9470	0.7763	0.9723
Mendonça and Campilho [8]	0.9452	0.7344	0.9764
Fraz et al. [6]	0.9430	0.7152	0.9769
Zhang et al. [10]	0.9382	0.7120	0.9724
Martinez-Perez et al. [11]	0.9344	0.7246	0.9655
Yang et al. [12]	-	-	-
Proposed method*	0.9607	0.7654	0.9789

*2nd human observer as ground truth.

TABLE V
AVERAGE PERFORMANCE RESULTS FOR STARE DATABASE.
(PARAMETERS: $l = 19$; $t = 42$; $c = 8$; $s = 4$; $p = 52$).

Methodology	Accuracy	Sensitivity	Specificity
Proposed method	0.9568	0.6699	0.9797
Lam et al. [18]	0.9567	-	-
Zhang et al. [10]	0.9484	0.7177	0.9753
Fraz et al. [6]	0.9442	0.7311	0.9680
Mendonça and Campilho [8]	0.9440	0.6996	0.9730
Martinez-Perez et al. [11]	0.9410	0.7506	0.9569
2nd human observer	0.9348	0.8951	0.9384
Yang et al. [12]	-	-	-
Proposed method*	0.9406	0.6120	0.9787

*2nd human observer as ground truth.

We achieved the best average accuracy and specificity at DRIVE and STARE databases when compared to these methods. Our average sensitivity is slightly inferior to Mendonça and Campilho [8] on DRIVE. However, the sensitivity and specificity results were not provided in Lam et al. [18]. Furthermore, Yang et al. [12] do not exhibit any of these measures at all. The advantage of our method is the robustness to noise features, which most of the segmented non-vessel pixels are correctly true negative, indeed. It is shown in Table VI the additional performance measures for both databases.

TABLE VI
ADDITIONAL PERFORMANCE RESULTS.

Metric	Database	2nd human observer	Fraz et al.[6]	Proposed method
FPR	DRIVE	0.0277	-	0.0216
	STARE	0.0616	-	0.0020
FNR	DRIVE	0.2237	-	0.2676
	STARE	0.1049	-	0.2554
PPV	DRIVE	0.7756	0.8112	0.7675
	STARE	0.8950	0.7294	0.7190
NPV	DRIVE	0.9818	0.9600	0.9742
	STARE	0.9562	0.9700	0.9624
MCC	DRIVE	0.7700	0.7359	0.7245
	STARE	0.7316	0.6908	0.6901

As aforementioned, the developed method is effective to segment retinal blood vessels. Moreover, the ability to detect

non-vessel pixels is the strength of our work, as one can see in Table VI, in which lowest FPR rates were obtained. Even with the presence of noise and pathologies, which are responsible for false positive detections, our method showed robustness when compared to the 2nd human observer. However, Fraz et al. [6] did not report these measurements.

The obtained results from DRIVE and STARE databases can be seen in Figs. 5 and 6, respectively, as well as the 2nd and the 1st manual segmentation. The best cases occurs when there is a low presence of thin vessels, since the large vessels are segmented easily. Thus, the accuracy in this kind of image is high. Although our method is able to segment some thin vessels, this still remains a difficult task, resulting in lower accuracy and sensitivity rates, when there is a large number of thin vessels, as in other methods. Such behavior can also be observed in Tables IV and V. Concerning the segmentation from human observer, the 1st human observer segmented less thin vessels than 2nd human observer at DRIVE while in STARE, 2nd human observer segmented more thin vessels than first one. Thus, the accuracy and sensitivity values increase slightly when adopting the specialist that segmented less thin vessels as ground truth. Moreover, the poor quality of STARE in comparison to DRIVE contributes to inferior results in that database.

VI. CONCLUSIONS AND FUTURE WORKS

An automated method for blood vessel segmentation in retinal fundus images using the combination of a morphological and topological extractors was presented in this paper. The morphological extractor was employed to extract the maximum pixels belonging to the vessel tree while the topological one was applied to ensure the topological vessel properties and connectivity. After we combined these two vessel trees, we smoothed the vessel borders and removed spurious objects, aiming to get a more accurate retinal vessel tree. The methodology has been validated in two widely used databases, namely, DRIVE and STARE, and has been compared against others methods found at literature. In addition to the high accuracy and specificity metric values obtained, our proposal can easily adjust itself to other databases by setting a few parameters, such as the top-hat threshold, contrast of skeletonization algorithm and the area size of the objects to be removed at the final step. These adjustments provide an effective way to increase the segmentation performance according to the database features. The development of a technique that can extract a large number of thin vessels, increasing the sensitivity and the application of the method on others databases are the topics of future works.

REFERENCES

- [1] P. Mitchell, H. Leung, J. J. Wang, E. Roctchina, A. J. Lee, T. Y. Wong, and R. Klein, "Retinal vessel diameter and open-angle glaucoma: the blue mountains eye study," *Ophthalmology*, vol. 112, no. 2, pp. 245–250, 2005.
- [2] R. Bernardes, P. Serranho, and C. Lobo, "Digital ocular fundus imaging: a review," *Ophthalmologica*, vol. 226, no. 4, pp. 161–181, 2011.

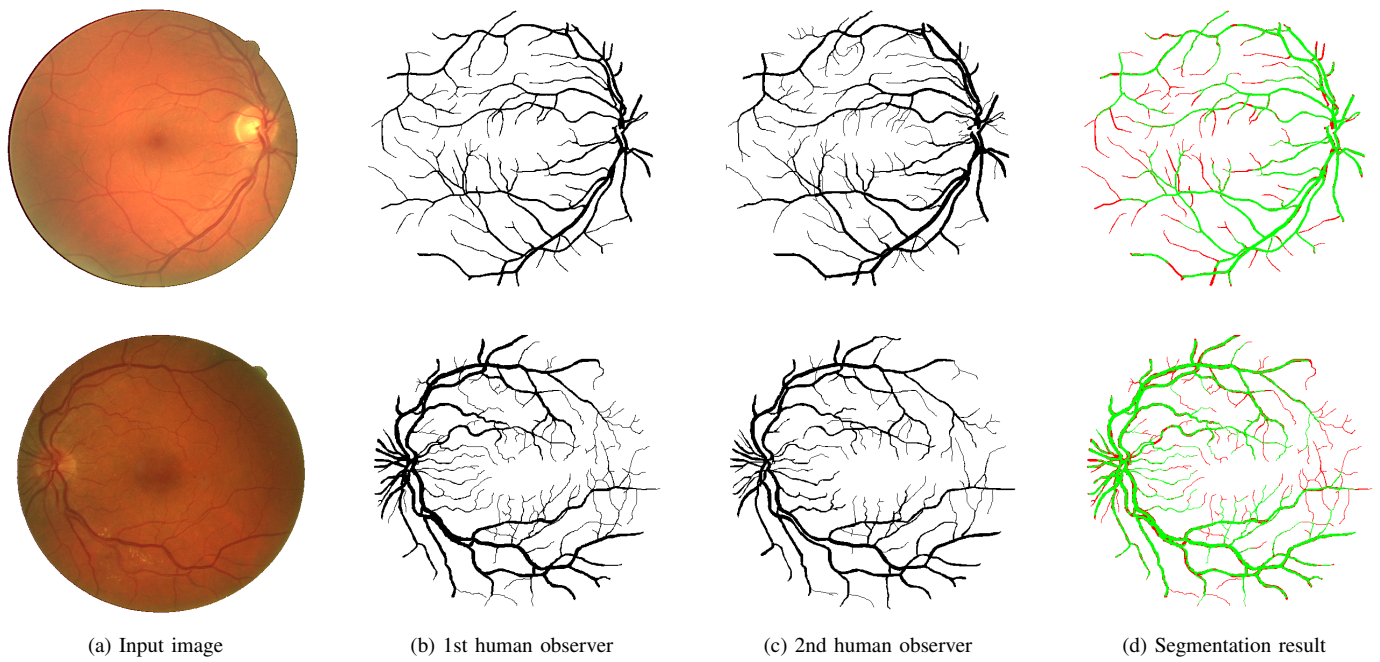


Fig. 5. The original images (a), the ground truth images (b), the outputs from the 2nd human observer (c), and our proposal (d), respectively, for the DRIVE database

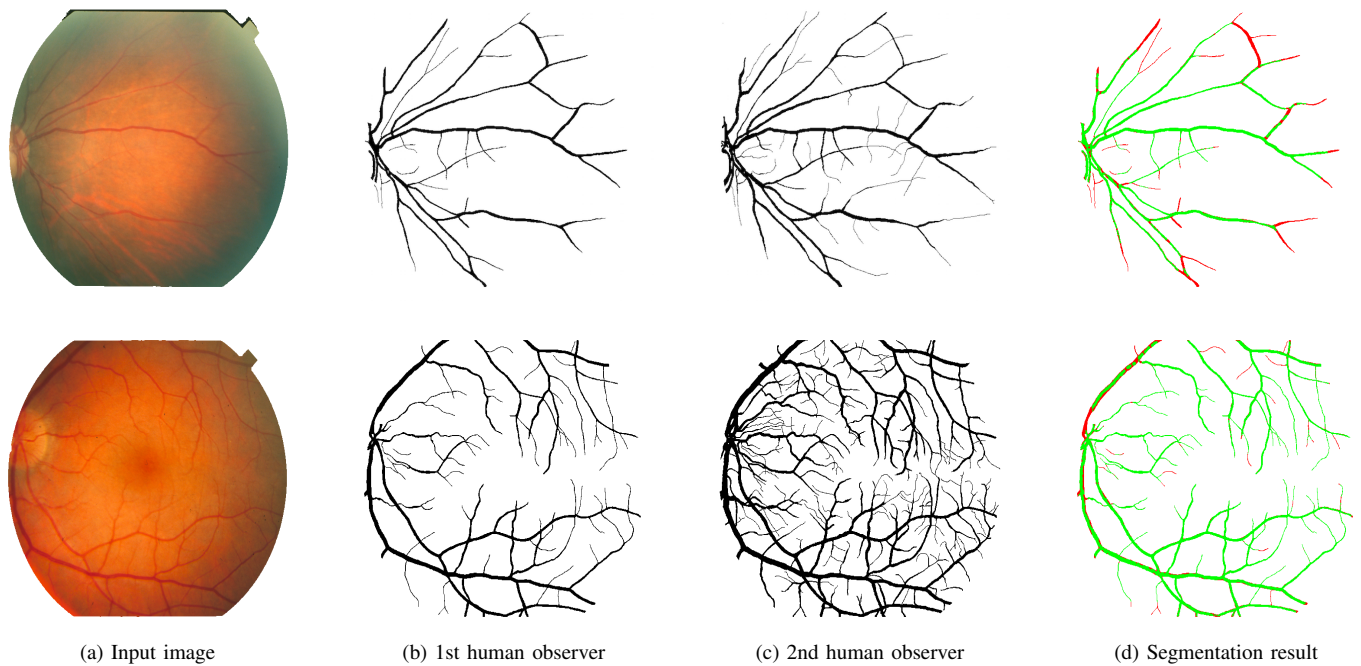


Fig. 6. The original images (a), the ground truth images (b), the outputs from the 2nd human observer (c), and our proposal (d), respectively, for the STARE database

- [3] M. M. Fraz, S. Barman, P. Remagnino, A. Hoppe, A. Basit, B. Uyyanonvara, A. R. Rudnicka, and C. G. Owen, "An approach to localize the retinal blood vessels using bit planes and centerline detection," *Computer methods and programs in biomedicine*, vol. 108, no. 2, pp. 600–616, 2012.
- [4] J. Staal, M. D. Abràmoff, M. Niemeijer, M. Viergever, B. Van Ginneken *et al.*, "Ridge-based vessel segmentation in color images of the retina," *Medical Imaging, IEEE Transactions on*, vol. 23, no. 4, pp. 501–509, 2004.
- [5] S. W. Franklin and S. E. Rajan, "Computerized screening of diabetic retinopathy employing blood vessel segmentation in retinal images," *Biocybernetics and Biomedical Engineering*, vol. 34, no. 2, pp. 117–124, 2014.
- [6] M. M. Fraz, P. Remagnino, A. Hoppe, B. Uyyanonvara, A. R. Rudnicka, C. G. Owen, and S. A. Barman, "Blood vessel segmentation methodologies in retinal images—a survey," *Computer methods and programs in biomedicine*, vol. 108, no. 1, pp. 407–433, 2012.
- [7] Y. Hou, "Automatic segmentation of retinal blood vessels based on improved multiscale line detection," *Journal of Computing Science and Engineering*, vol. 8, no. 2, pp. 119–128, 2014.
- [8] A. M. Mendonça and A. Campilho, "Segmentation of retinal blood vessels by combining the detection of centerlines and morphological reconstruction," *Medical Imaging, IEEE Transactions on*, vol. 25, no. 9, pp. 1200–1213, 2006.
- [9] Z. Xiao, M. Adel, and S. Bourennane, "Bayesian method with spatial constraint for retinal vessel segmentation," *Computational and mathematical methods in medicine*, vol. 2013, 2013.
- [10] B. Zhang, L. Zhang, L. Zhang, and F. Karray, "Retinal vessel extraction by matched filter with first-order derivative of gaussian," *Computers in biology and medicine*, vol. 40, no. 4, pp. 438–445, 2010.
- [11] M. E. Martínez-Pérez, A. D. Hughes, S. A. Thom, A. A. Bharath, and K. H. Parker, "Segmentation of blood vessels from red-free and fluorescein retinal images," *Medical image analysis*, vol. 11, no. 1, pp. 47–61, 2007.
- [12] Y. Yang, S. Huang, and N. Rao, "An automatic hybrid method for retinal blood vessel extraction," *International Journal of Applied Mathematics and Computer Science*, vol. 18, no. 3, pp. 399–407, 2008.
- [13] K. K. Delibasis, A. I. Kechriniotis, C. Tsonos, and N. Assimakis, "Automatic model-based tracing algorithm for vessel segmentation and diameter estimation," *Computer methods and programs in biomedicine*, vol. 100, no. 2, pp. 108–122, 2010.
- [14] D. Marín, A. Aquino, M. E. Gegúndez-Arias, and J. M. Bravo, "A new supervised method for blood vessel segmentation in retinal images by using gray-level and moment invariants-based features," *Medical Imaging, IEEE Transactions on*, vol. 30, no. 1, pp. 146–158, 2011.
- [15] E. Ricci and R. Perfetti, "Retinal blood vessel segmentation using line operators and support vector classification," *Medical Imaging, IEEE Transactions on*, vol. 26, no. 10, pp. 1357–1365, 2007.
- [16] C. Sinthanayothin, J. F. Boyce, H. L. Cook, and T. H. Williamson, "Automated localisation of the optic disc, fovea, and retinal blood vessels from digital colour fundus images," *British Journal of Ophthalmology*, vol. 83, no. 8, pp. 902–910, 1999.
- [17] J. V. Soares, J. J. Leandro, R. M. Cesar Jr, H. F. Jelinek, and M. J. Cree, "Retinal vessel segmentation using the 2-d gabor wavelet and supervised classification," *Medical Imaging, IEEE Transactions on*, vol. 25, no. 9, pp. 1214–1222, 2006.
- [18] B. S. Lam, Y. Gao, and A. W.-C. Liew, "General retinal vessel segmentation using regularization-based multiconcavity modeling," *Medical Imaging, IEEE Transactions on*, vol. 29, no. 7, pp. 1369–1381, 2010.
- [19] M. P. Friedman, *Handbook of perception*. Academic Press, 1978, vol. 1.
- [20] R. Aramesh and K. Faez, "A new method for segmentation of retinal blood vessels using morphological image processing technique," *International Journal of Advanced Studies in Computer Science and Engineering*, vol. 3, no. 1, 2014.
- [21] M. Couprie, N. Bezerre, and G. Bertrand, "A parallel thinning algorithm for grayscale images," in *Discrete Geometry for Computer Imagery*. Springer, 2013, pp. 71–82.
- [22] J. Rodrigues and F. Bezerre, "Retinal vessel segmentation using crest lines and morphological operations," *International Journal of Scientific Engineering Research*, vol. 6, no. 9, pp. 1277–1281, 2015.
- [23] P. Soille, *Morphological image analysis: principles and applications*. Springer Science & Business Media, 2013.
- [24] M. Niemeijer, J. Staal, B. Ginneken, M. Loog, and M. Abramoff, "Drive: digital retinal images for vessel extraction," 2004.
- [25] A. Hoover, V. Kouznetsova, and M. Goldbaum, "Locating blood vessels in retinal images by piecewise threshold probing of a matched filter response," *Medical Imaging, IEEE Transactions on*, vol. 19, no. 3, pp. 203–210, 2000.
- [26] D. Gadriye, G. Khandale, and R. Nawkhare, "System for diagnosis of diabetic retinopathy using neural network," *International Journal of Technical Research and Applications*, vol. 4, no. 2, pp. 76–80, 2014.